J. Plasma Phys. (2025), *vol*. 91, E122
 doi:10.1017/S0022377825100652

Variational quantum simulation of the Fokker–Planck equation applied to quantum radiation reaction

Óscar Amaro[1], Lucas Ivan Iñigo Gamiz[1] and Marija Vranic[1]

[1]GoLP/Instituto de Plasma e Fusão Nuclear, Instituto Superior Técnico, Universidade de Lisboa, Lisbon, Portugal

Corresponding authors: Óscar Amaro, oscar.amaro@tecnico.ulisboa.pt; Marija Vranic, marija.vranic@tecnico.ulisboa.pt

(Received 26 February 2025; revision received 24 June 2025; accepted 25 June 2025)

Near-future experiments with Petawatt class lasers are expected to produce a high flux of gamma-ray photons and electron–positron pairs through strong field quantum electrodynamical processes. Simulations of the expected regime of laser–matter interaction are computationally intensive due to the disparity of the spatial and temporal scales, and because quantum and classical descriptions need to be accounted for simultaneously (classical for collective effects and quantum for nearly instantaneous events of hard photon emission and pair creation). We study the stochastic cooling of an electron beam in a strong, constant, uniform magnetic field, both its particle distribution functions and their energy momenta. We start by obtaining approximate closed-form analytical solutions to the relevant observables. Then, we apply the quantum-hybrid variational quantum imaginary time evolution to the Fokker–Planck equation describing this process and compare it against theory and results from particle-in-cell simulations and classical partial differential equation solvers, showing good agreement. This work will be useful as a first step towards quantum simulation of plasma physics scenarios where diffusion processes are important, particularly in strong electromagnetic fields.

Key words: intense particle beams, quantum plasma

1. Introduction

Strong-field quantum electrodynamics (SFQED) studies the interaction between matter and intense electromagnetic fields. In recent years, there has been a growing interest in this area due to the availability of high-intensity laser sources, which enable the exploration of novel physical phenomena, with experiments being planned for the near future at ELI Extreme Light Infrastructure, Apollon (Papadopoulos, Zou & Le Blanc 2016), CoReLS (Yoon *et al*. 2019), FACET-II (Meuren *et al*. 2020), LUXE (Abramowicz *et al*. 2019, 2021), XCELS (Mukhin *et al*. 2021), ZEUS, NSF-OPAL, HIBEF, among others. Many of the proposed experimental set-ups feature scattering of intense, focused laser pulses with either relativistic electron beams or high-energy photons.

Some experimental evidence for radiation reaction has been observed (Cole *et al*. 2018; Poder *et al*. 2018; Los *et al*. 2024). However, additional theoretical and numerical studies are needed to understand the effects of 'non-ideal' experimental conditions such as laser jitter, probe beam emittance, synchronisation of the collision, etc. In the future, better control over these parameters will allow precision studies of the radiation reaction, that is, the recoil on the charged particles that emit high-energy photons and electron–positron production in the lab, among other processes. These can then be applied in physics models of plasmas in extreme astrophysical environments, such as black holes and pulsar magnetospheres (Timokhin 2010; Medin & Lai 2010; Uzdensky & Rightley 2014; Cruz *et al*. 2021; Schoeffler *et al*. 2023).

While current laser technology allows us to test strong-field plasma physics in a 'semi-classical' regime, next-gen laser facilities will require exploring the fully non-perturbative quantum dynamics of fermions, high-energy photons and the laser field. This regime is expected to require first-principles simulation techniques, thus putting constraints on the more standard particle-in-cell simulations, even if including Monte Carlo routines for the quantum processes. It is thus important to begin translating known simulation methods into the quantum computing framework.

Quantum computing has the potential to handle the complexity of the many-body-physics dynamics in these extreme plasmas. Recently, the plasma physics community has started to adapt standard plasma set-ups and theory to the quantum algorithmic framework (Dodin & Startsev 2021; Amaro & Cruz 2023; Joseph *et al*. 2023). More specifically, the intersection between plasma physics, quantum field theory and quantum computing has only recently started to be explored (Shi, Qin & Fisch 2021).

In this work, we aim to address some of these questions, first by deriving approximate particle distributions and benchmarking with the particle-in-cell code `OSIRIS` (Fonseca *et al*. 2002) that describes QED effects with a Monte Carlo routine to simulate quantum events and has already been tested in this regime (Vranic *et al*. 2016) and later by applying a hybrid quantum algorithm to the simulation of a Fokker–Planck equation relevant for SFQED. We choose the simplest possible field configuration, a strong constant magnetic field background, that could be generalised in the future. We start with a relativistic electron beam, which propagates and loses energy to radiation. We follow the evolution of the electron distribution function over time, accounting for the stochastic nature of the quantum emission.

While prior work (e.g. Kubo *et al*. 2021) suggests that hybrid quantum algorithms could provide sampling efficiency benefits for more complex stochastic differential equations (SDEs) – such as those with high dimensionality or intricate observables relevant to finance and physics – even within the NISQ era, this implementation does not outperform classical methods at this point. As such, our primary aim is not to claim a quantum advantage, but to present a proof of concept demonstrating that quantum hardware can, in principle, be used to simulate SDEs with applications to plasma physics.

This manuscript is structured as follows. In § 2, we describe the set-up of an electron beam propagating perpendicularly to a strong magnetic field and radiating energy in the form of photons in the so-called semi-classical regime. We introduce the Fokker–Planck equation and derive solutions for the evolution of the distribution function and the first two energy moments, with details in Appendix B. In § 3, we describe the quantum variational simulation of the Fokker–Planck equation, the choice of ansatz and the numerical evolution of the parameters using variational quantum imaginary time evolution (VarQITE). Conclusions are given in § 4.

https://doi.org/10.1017/S0022377825100652 Published online by Cambridge University Press

2. Fokker–Planck equation for quantum radiation reaction

In this section, we introduce the main parameters for the physical set-up, the Fokker–Planck equation describing the interaction of electrons with an intense magnetic field, and approximate formulae for the first two moments of the electron distribution functions. The importance of quantum effects of relativistic particles in strong fields is controlled by the quantum nonlinearity parameters, which for leptons and photons are given by

$$\chi \equiv \frac{\sqrt{(p_\mu F^{\mu\nu})^2}}{E_S\, mc}, \quad \chi_\gamma \equiv \frac{\sqrt{(\hbar k_\mu F^{\mu\nu})^2}}{E_S\, mc}, \tag{2.1}$$

where m is the electron mass, c is the speed of light in vacuum, $E_S = m^2c^3/(e\hbar) = 1.32 \times 10^{18}$ V m^{-1} and $B_S = E_S/c = 4.41 \times 10^9$ T represent the critical Schwinger electric and magnetic fields, e is the elementary electric charge, $\hbar$ is the reduced Planck constant, $F_{\mu\nu}$ is the electromagnetic field tensor, and p_μ, k_μ are the leptonic and photonic 4-momenta. In the case of a relativistic electron moving perpendicularly to a strong, uniform and constant magnetic field, we have

$$\chi = \gamma B/B_S. \tag{2.2}$$

The electron distribution function $f = \mathrm{d}N/\mathrm{d}\gamma$, that is, the number of electrons $\mathrm{d}N$ per interval of energy $\mathrm{d}\gamma$, evolves through a Fokker–Planck equation describing stochastic energy losses

$$\frac{\partial f(t,\gamma)}{\partial t} = \frac{\partial}{\partial \gamma}\left[-(\mathcal{A}f) + \frac{1}{2}\frac{\partial}{\partial \gamma}(\mathcal{B}f)\right]. \tag{2.3}$$

This is the partial differential equation that will be simulated through a quantum algorithm in a later section. The scalar drift and diffusion space-dependent terms can be approximated in the $\chi \ll 1$ regime as

$$\mathcal{A} \sim \frac{2}{3}\frac{\alpha mc^2}{\hbar}\chi^2 = a\,\gamma^2, \quad \mathcal{B} \sim \frac{55}{24\sqrt{3}}\frac{\alpha mc^2}{\hbar}\gamma\,\chi^3 = \frac{b^2}{2}\,\gamma^4, \tag{2.4}$$

where $a \equiv 2\alpha k^2/(3\tau_c)$, $\alpha \equiv e^2/(\hbar c)$ is the fine structure constant and $b \equiv \sqrt{55\alpha k^3/(12\sqrt{3}\tau_c)}$, with Compton time $\tau_c \equiv \hbar/(mc^2)$ and normalised magnetic field $k \equiv B/B_S$ (Neitz & Di Piazza 2013; Vranic *et al*. 2016). In general, there are no closed-form solutions for the electron distribution function valid in all regimes of quantum nonlinearity χ. Further details on the theory of quantum radiation reaction are presented in Appendix B.

2.1. *Evolution of the electron distribution function*

In this section, we use the classical approach of simulating the particle motion coupled with Monte Carlo routines to account for the hard-photon emission and quantum radiation reaction. As such, it can describe the evolution of the electron distribution, including the energy loss and quantum stochasticity-induced widening of the spectrum.

In OSIRIS, the Monte Carlo (MC) subroutine is added to the particle-in-cell algorithmic loop between the steps of integration of equations of motion (e.g. the Lorentz force) and the current deposition on the grid. First, the total probability

https://doi.org/10.1017/S0022377825100652 Published online by Cambridge University Press

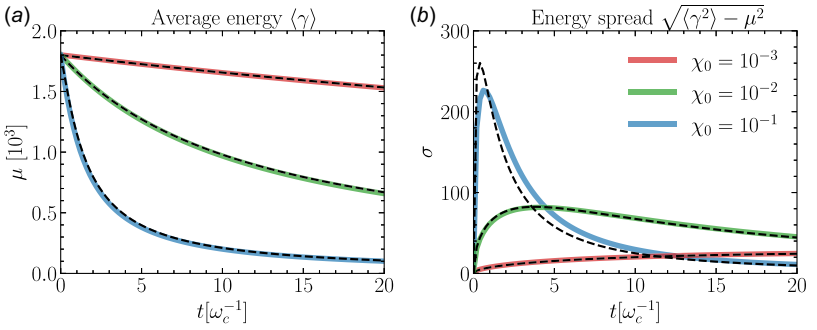

FIGURE 1. Evolution of the moments of the distribution function of electrons in a constant magnetic field. (*a*) Average energy and (*b*) spread for zero initial spread $\sigma_0 = 0$ (monoenergetic beam of electrons). Dashed lines , theory; coloured lines, OSIRIS simulation results.

of the cross-section for the MC process to occur within the simulation time step is computed for all particles. If this probability is above a random uniformly generated value in the interval [0, 1], then the process is assumed to have occurred. For the particles in which this happens, a second random number is generated to sample the energy of the generated particle from the corresponding differential cross-section. The new particles with their respective energies will then be responsible for updating the currents on the grid. The PIC loop then proceeds as usual.

In the $\chi \ll 1$ regime, an initially narrow distribution with energy γ_0 retains an approximately Gaussian shape throughout the interaction. Following the approach of Torgrimsson (2024*a*,*b*) and Blackburn (2024), which is based on a perturbative expansion in χ, the mean energy $\mu = \langle\gamma\rangle = \int \gamma f \, \mathrm{d}\gamma$ and energy spread $\sigma^2 = \int (\gamma - \mu)^2 f \, \mathrm{d}\gamma$ in a constant magnetic field can be obtained as

$$\frac{\mu}{\gamma_0} \sim \frac{1}{1 + 2R_c t/3} + \frac{165\chi_0}{8\sqrt{3}(1 + 2/3R_c t)^2} \log\left(1 + \frac{2R_c t}{3}\right), \tag{2.5}$$

$$\frac{\sigma^2}{\gamma_0^2} \sim \frac{\sigma_0^2 + 55R_c\chi_0 t/(24\sqrt{3})}{(1 + 2R_c t/3)^4}, \tag{2.6}$$

where $R_c \equiv \alpha\, b_0\, \chi_0$ is the classical radiation reaction parameter, $b_0 \equiv eB/(m\,\omega_c)$ is an adimensional normalised magnetic field and $\omega_c \equiv eB/(m\gamma_0)$ is the synchrotron frequency. In our simulations, the time is normalised as $t \to t\,\omega_c$, and the average electron energy and normalised magnetic field are $\gamma_0 = b_0 = 1800$. From (2.6), the maximum energy spread occurs approximately at $t \sim 1/(2R_c)$ for $\sigma_{max} \sim 3^{5/4}\sqrt{55}/64\,\gamma_0\sqrt{\chi_0}$, which recovers the scaling derived by Vranic *et al*. (2016). To test the validity of these analytical expressions, we run 1-D3V simulations with an electron beam moving perpendicular to the constant, uniform magnetic field vector. The time step is $\mathrm{d}t = 0.001\,\omega_c^{-1}$, the cell size $\mathrm{d}x = 0.049\,c/\omega_c$, and the normalising frequencies and external magnetic field values are chosen to enforce $\chi_0 = \{10^{-3}, 10^{-2}, 10^{-1}\}$.

In figure 1, we show results from OSIRIS MC simulations for different values of the external magnetic field (different values of initial, average χ_0), and the moments from (2.5) and (2.6). The latter expressions capture the simulation results well, with some loss of accuracy for $\chi_0 = 10^{-1}$.

https://doi.org/10.1017/S0022377825100652 Published online by Cambridge University Press

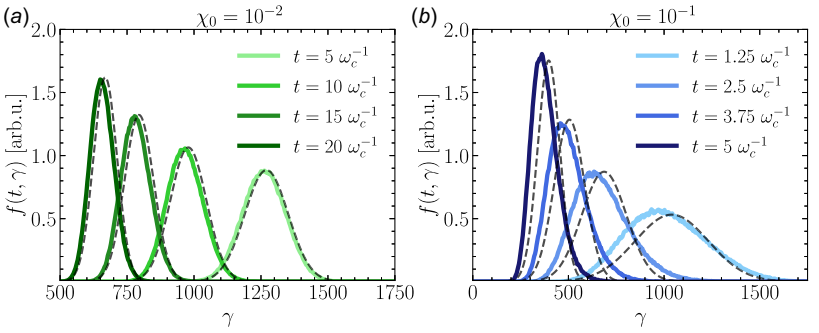

FIGURE 2. Snapshots of the distribution functions, taking the analytical formulas for the mean energy and energy spread ((2.5) and (2.6)) for $\chi_0 = \{10^{-2}, 10^{-1}\}$. Dashed lines, Gaussian approximation; coloured lines, OSIRIS simulation results. For $\chi_0 = 10^{-1}$, there is a visible deviation from the Gaussian approximation.

In figure 2, we show snapshots of Gaussian distribution functions using the parameters (μ, σ) from (2.5) and energy histograms from the OSIRIS MC simulations. Although for $\chi_0 = 10^{-2}$ there is good agreement with simulation results, it is clear that in the higher $\chi_0 = 10^{-1}$ regime, the validity of the Gaussian functional approximation is lost, even though the moments (μ, σ) predicted analytically are close to what was obtained in the simulation. This deviation is due to an increased skewness of the distributions. These results will serve as a 'ground truth' for testing the quantum algorithm presented in the following section.

3. Variational quantum simulation

In this section, we introduce the variational quantum simulation (VQS) method employed in our study. Quantum computing holds the potential to revolutionise simulations of complex systems, encompassing both quantum many-body problems and certain classical physics phenomena. The fundamental unit of quantum computation is the qubit, which, unlike a classical bit, can exist in a superposition of states described by $|\psi\rangle = a_0|0\rangle + a_1|1\rangle$, where a_0 and a_1 are complex amplitudes satisfying the normalisation condition $|a_0|^2 + |a_1|^2 = 1$ (Nielsen & Chuang 2010). When multiple qubits are combined into a register, their joint state can exhibit entanglement – a uniquely quantum mechanical correlation that leads to an exponentially large state space, challenging to simulate efficiently on classical computers. In this work, we use the big-endian convention – the left-most qubit is the most significant.

Currently, quantum computers are in the noisy intermediate-scale quantum (NISQ) era (Preskill 2018), characterised by devices that contain a moderate number of qubits, but are susceptible to errors and decoherence. These limitations restrict the depth and complexity of quantum circuits that can be reliably executed, posing significant challenges for implementing algorithms requiring long coherence times and high gate fidelities.

To address these challenges, variational quantum circuits (VQCs) have emerged as a promising approach suitable for NISQ devices. VQCs are hybrid quantum-classical algorithms that employ parametrised quantum circuits optimised using classical optimisation routines to minimise a cost function, typically the expectation value of an observable. This method reduces the required circuit depth by offloading part of the computational workload to classical processors, making it more practical for current

https://doi.org/10.1017/S0022377825100652 Published online by Cambridge University Press

quantum hardware. Variational quantum algorithms have found applications across various fields, including quantum chemistry (Peruzzo *et al*. 2014), material science (Liu, Li & Yang 2024), biology (Robert *et al*. 2021) and others (Farhi, Goldstone & Gutmann 2014). By carefully designing the variational circuits and selecting appropriate ansätze, VQCs leverage the expressive power of quantum systems while operating within the practical constraints of NISQ devices. Extracting meaningful information from the exponentially large quantum state space necessitates meticulous selection and measurement of observables, as quantum measurements yield probabilistic outcomes that collapse the superposed state. The variational approach thus provides a flexible and adaptive framework for quantum simulation, contributing significantly to the advancement of quantum computing applications in science and engineering.

In plasma physics, several phenomena of interest are intrinsically dissipative. Since dissipation is an irreversible process, this is challenging to model on quantum computers. Engel, Smith & Parker (2019) studied Landau damping on a quantum framework using a linearised version of the Vlasov equation. Despite the name 'damping', the energy of the system is not lost, but rather transferred from the electric field to the particle distribution function in a reversible/unitary manner. Vissers & Bouten (2019) studied a 'quantum stochastic' process of a laser driven two-level atom interacting with an electromagnetic field. However, a procedure to generalise beyond two-level systems is not provided. Kubo *et al*. (2021) proposed a partial/stochastic differential equation (PDE/SDE) solver of the Fokker–Planck equation in the form of an Itô-process in a quantum variational framework. This approach was then generalised by Alghassi *et al*. (2022) through the Feynman−Kac formula, which unifies the heat, Schrödinger, Black−Scholes, Hamilton−Jacobi and Fokker–Planck equations under this formalism.

The expressibility of variational quantum circuits is one of the most important figures of merit in the field of VQS. It is defined as the ability of the variational quantum circuit to produce a variety of quantum wavefunctions – the higher this value is means the larger the fraction of the Hilbert space is that is accessible through the circuit. This metric has been studied in detail, and heuristics on which architectures one can reach higher expressibility have been discussed (Sim, Johnson & Aspuru-Guzik 2019). However, few proofs or universal rules have been derived so far. In the case of Kubo *et al*. (2021), the authors suggest using an ansatz with only R_Y and CNOT quantum gates, which permits only real-valued amplitudes of the wavefunction, but it also allows for negative values. Dasgupta & Paine (2022) suggest an architecture to enforce even-symmetry of the real-valued wavefunction around the middle of the computational basis representation. Endo *et al*. (2020) based the motivation for using compact variational circuits on the intuition that the dynamics of the physical system only span low energy states and therefore is limited to a small portion of the entire Hilbert space.

In this work, we consider wave/distribution functions that are well localised in space, but can have a mean position/energy that can be off-centred, that is, not located at the middle of the computational basis $|01\ldots1\rangle$, $|10\ldots0\rangle$. For this, we use a quantum circuit which simulates the advection equation based on the finite differences operator as presented by Sato *et al*. (2024). This operation can be used to shift the entire wavefunction, which allows the exploration of a larger space of states.

In figure 3, we show the hybrid quantum optimisation loop. First, at a time step t, a quantum wavefunction is produced by the quantum circuit, where some of the

https://doi.org/10.1017/S0022377825100652 Published online by Cambridge University Press

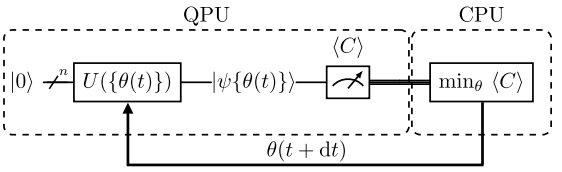

FIGURE 3. Variational quantum algorithm. From the quantum processing unit (QPU), we measure a cost function, from which the variational parameters are optimised in the CPU.

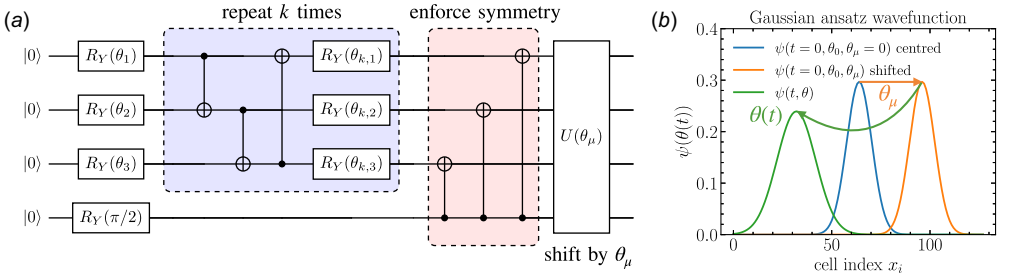

FIGURE 4. (*a*) Variational ansatz used in this work. Only four qubits are shown for simplicity. The blue box represents a variational block that can be repeated k times. The red box represents the enforcing of even-symmetry on the wavefunction. In the last step, the advection operator is applied to displace the wavefunction from the middle of the grid. (*b*) Sketch of the typical evolution of the wavefunction.

quantum unitary operations are parametrised by values $\theta(t)$. Then, a cost function $\langle C \rangle$ is measured from the quantum circuit and minimised/updated through an algorithm run on a classical device. The new parameters are then fed-back to the quantum circuit to produce the wavefunction for the next time step $\theta(t + \mathrm{d}t)$. The finite-difference approximation to the Fokker–Planck operator is of the trinomial type, where any grid cell at any time step is only influenced by its two close neighbouring cells. Higher-order finite-difference schemes are possible to apply, but require more complex algorithms.

3.1. *Variational ansatz*

In figure 4, we show the ansatz used in this work. In the first variational block (blue), we produce a real-valued wavefunction using parameters $\boldsymbol{\theta}$ and gates $\mathrm{CNOT} - R_Y$ in a ring structure (the qubit $n-1$ connects with the first qubit). This block can be repeated to increase the expressibility of the ansatz. The second block (red) consists of enforcing even-symmetry on the wavefunction; that is, the amplitudes have a mirror symmetry around half of the computational basis $\psi_{0111} = \psi_{1000}$, $\psi_{0000} = \psi_{1111}$. If, instead, we apply an angle $-\pi/2$ on the R_Y gate acting on the last qubit, then the wavefunction becomes odd instead of even-symmetric. At $t = 0$, we fit these parameters so that the wavefunction has an approximate Gaussian shape with a prescribed standard deviation σ. In this way, the parameters $\boldsymbol{\theta}$ are implicit functions of σ.

In the final step of the quantum circuit, we apply the advection operator $e^{-i\theta_\mu \partial_x}$, which is a unitary operation, and which translates the entire wavefunction by some quantity θ_μ. Sato *et al.* (2024) provide a quantum circuit for the finite-difference

https://doi.org/10.1017/S0022377825100652 Published online by Cambridge University Press

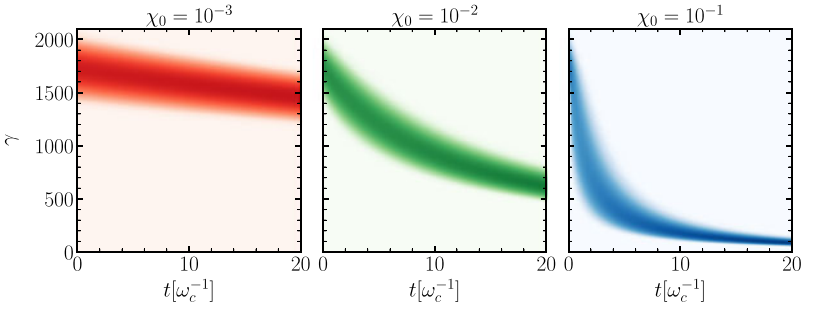

FIGURE 5. Evolution of electron distribution functions from OSIRIS simulations for different initial average χ_0 values and spread $\sigma_0 = 90$. In all cases, the maximum simulation time is $20\,\omega_c^{-1}$.

version of the first order of $\partial_x \sim (s_+ - s_-)/2$, where $s_+ = s_-^\dagger$ is the operator that shifts the wavefunction one cell to the right (left) with a periodic boundary condition. Here, we use the second order of this finite-difference operator to enforce higher fidelity of the translation.

3.2. *Variational quantum simulation of the Fokker–Planck equation*

In figure 5, we show the complete evolution of the distribution functions for $\mu_0 = 1800$, $\sigma_0 = 90$ from OSIRIS Monte Carlo simulations, following the same set-up parameters as Niel *et al*. (2018), which we take as being the 'ground-truth' benchmark. In these simulations, the electrons can be seen to cool down quicker for higher χ_0, and the distribution functions occupy different fractions of the energy domain throughout the evolution, thus having different requirements on the resolution for the energy grid.

The VQS algorithm maps the dynamics of the quantum state, (2.3), to those of the variational parameters $\theta(t)$ of the ansatz. The mapping is performed using McLachlan's variational principle (MVP) (McLachlan 1964; Endo *et al*. 2020). Using the same notation as Kubo *et al*. (2021), the unitary quantum circuit from figure 4 produces a wavefunction $|v\{\boldsymbol{\theta}(t)\}\rangle$. However, diffusive processes generally do not preserve the L_2 norm, that is, $\partial_t \int |v|^2 \,\mathrm{d}x \neq 0$. Therefore, it is useful to define an overall variational wavefunction $|\tilde{v}\{\boldsymbol{\theta}(t)\}\rangle = \alpha(t)\,|v\{\boldsymbol{\theta}(t)\}\rangle$, where $\alpha(t)$ is a (classical) normalisation parameter. If the temporal resolution is sufficiently high and the ansatz sufficiently expressive, the MVP method evolves the variational parameters such that the correct dynamics is enforced through

$$\min_{\theta(t)} \left\| \frac{\mathrm{d}}{\mathrm{d}t} |\tilde{v}\{\boldsymbol{\theta}(t)\}\rangle - \hat{L}\,|\tilde{v}\{\boldsymbol{\theta}(t)\}\rangle \right\|, \tag{3.1}$$

where $\hat{L}$ is a linear operator that generates the evolution of the system. At each time step, the following matrix equation needs to be solved on a classical computer

$$M_{k,j}\,\dot{\theta}_j = V_k, \tag{3.2}$$

where

$$M_{k,j} \equiv \mathrm{Re}\left(\frac{\partial \langle \tilde{v}\{\theta(t)\}|}{\partial \theta_k} \frac{\partial |\tilde{v}\{\theta(t)\}\rangle}{\partial \theta_j} \right), \quad V_k \equiv \mathrm{Re}\left(\frac{\partial \langle \tilde{v}\{\theta(t)\}|}{\partial \theta_k} \hat{L} |\tilde{v}\{\theta(t)\}\rangle \right) \tag{3.3}$$

https://doi.org/10.1017/S0022377825100652 Published online by Cambridge University Press

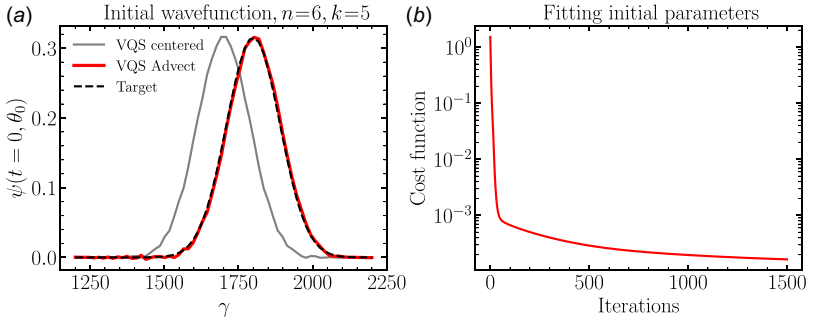

FIGURE 6. Fitting of the initial wavefunction for $\chi_0 = 10^{-3}$, $n = 6$ qubits and $k = 5$ layers of variational parameters. (*a*) A centred wavefunction is obtained through fitting the variational parameters. (*b*) Evolution of the cost function as the optimiser converges on a good approximation of the target wavefunction.

are quantities that can be obtained efficiently through dedicated quantum circuits. One advantage of this method, if run on a quantum device, is that one does not need to have access to the full amplitudes of the wavefunction. Instead, only the variational parameters need to be tracked and their evolution is obtained through efficient measurement of a few observables. Whereas the $M_{k,j}$ only depend on the chosen ansatz, the V_k elements depend on both the ansatz and the particular Fokker–Planck equation operators (in this case, (2.3)). In this work, we classically simulate the retrieval of these quantities through numerical differentiation and integration of the wavefunction using `Numpy` (Harris *et al*. 2020). A complete example of application of analytical solution to the heat equation using this variational method is presented in Appendix A.

As previously explained, we first optimise the parameters (except for θ_μ, which we keep fixed) using a cost function $C = ||\psi(\theta) - \psi_{target}||^2$ (mean-squared error). We choose a number of iteration steps such that the cost function has decreased significantly and converged such that the quantum variational ansatz produces the centred target distribution (see figure 6). After this, we apply the advection step by changing the parameter θ_μ to match the initial mean value of the distribution on the energy grid.

The number of variational parameters depends indirectly on the value of χ. A higher initial χ_0 corresponds to entering deeper into the quantum regime of radiation reaction, where the resulting electron distribution becomes increasingly asymmetric and skewed. This symmetry breaking typically requires a larger number of variational parameters (or circuit layers) to be accurately captured within our ansatz. Furthermore, for a given fixed simulation time, a higher χ will lead to higher energy loss, and consequently requires a wider grid domain. From empirical parameter scans for different values of n and k, we find that, in practice, achieving good fidelity in reproducing the initial symmetric (Gaussian) distribution typically requires the number of layers k to scale approximately linearly with the number of qubits n, specifically in the range $k \sim n$ to $k \sim 2n$.

In figure 7, we show the VarQITE simulation of the distribution function for $\chi_0 = \{10^{-3}, 10^{-2}\}$, and results from solving the PDE with a classical algorithm. This PDE solver employs the same energy-grid discretisation as the VarQITE approach to provide a reference to which to compare. We use a forward Euler pusher in

https://doi.org/10.1017/S0022377825100652 Published online by Cambridge University Press

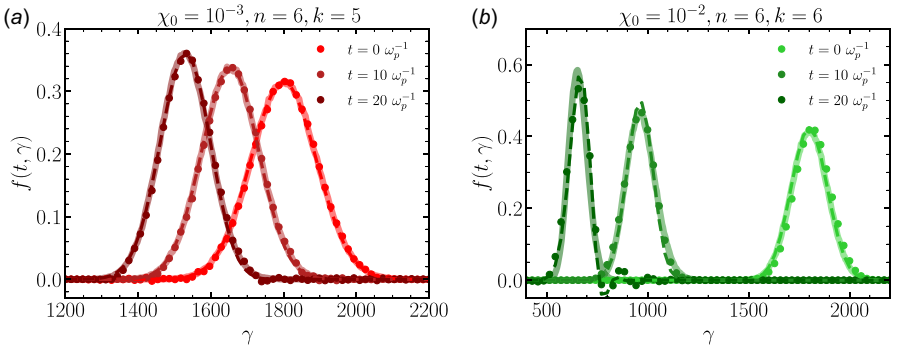

FIGURE 7. Evolution of electron distribution functions for $\chi_0 = \{10^{-3}, 10^{-2}\}$, for an initial spread in energy $\sigma_0 = 90$. Full line, OSIRIS simulation; dashed line, PDE solver; circles, VarQITE. In both cases, $n = 6$ qubits, while the number of layers is (*a*) $k = 5$ for $\chi_0 = 10^{-3}$ and (*b*) $k = 6$ for $\chi_0 = 10^{-2}$.

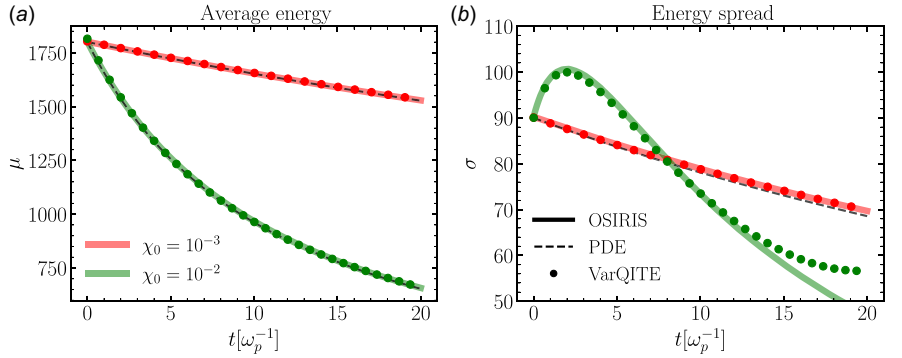

FIGURE 8. Evolution of the moments of the distribution functions obtained through VarQITE (circles) and compared against OSIRIS (lines). (*a*) First moment (mean), (*b*) second moment (spread). The number of layers for each case is the same as in figure 7.

time and a finite-difference scheme on the energy-grid, only accounting for nearest neighbour cells. The discretised versions of the $\partial_\gamma(\mathcal{A}f)$ advection and $0.5\,\partial_{\gamma\gamma}(\mathcal{B}f)$ diffusion operators are then the same between the approaches.

In figure 8, we show the evolution of the first two moments of the distribution functions. There is a general agreement of the quantum circuit results with the OSIRIS simulations. There is a small deviation due to finite grid resolution, which can be resolved by increasing the number of qubits.

In figure 9(*a*), we show the evolution of all the 27 variational parameters for the $\chi_0 = 10^{-3}$ case. The trajectories are smooth and some parameters have minimal deviations, which suggests that the ansatz is over-parametrised and can be made more efficient. Figure 9(*b*) shows the values of the mean energy computed from the wavefunction produced by the quantum variational ansatz against the variational parameter responsible for the translation $e^{-i\theta_\mu \partial_x}$, where a linear scaling between the two is visible.

https://doi.org/10.1017/S0022377825100652 Published online by Cambridge University Press

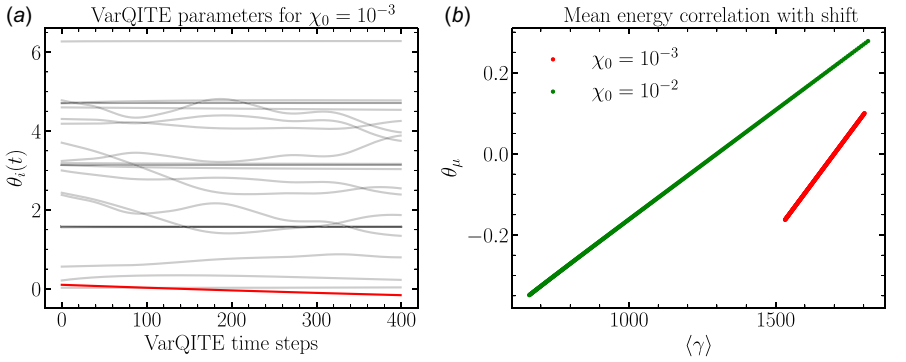

FIGURE 9. (*a*) Evolution of all variational parameters for $\chi_0 = 10^{-3}$, highlighting the 'average energy' parameter in red. (*b*) Linear correlation between average energy from the wavefunction and the parameter of the wavefunction translation.

3.3. *A note on the extraction of moments of the distribution function*

The global translation of the wavefunction is correlated with the average energy through a simple rescaling. Therefore, we would not need to measure the mean energy of the wavefunction because we could simply read this value from one of the variational parameters. This is only allowed because of our choice of a translated, even-symmetric wavefunction and would not be viable if the ansatz allowed for skewed distributions.

The average and variance of the energy can be measured efficiently (n Z_i and $n^2/2$ Z_iZ_j gates, respectively), with a Pauli-string decomposition of the observables:

$$\hat{x} = \frac{1}{2}(2^n - 1)\, I - \frac{1}{2}\sum_{i=0}^{n-1} 2^{n-i-1} Z_i, \tag{3.4}$$

$$\hat{x}^2 = \left(a^2 + \sum_{i=0}^{n-1} b_i^2\right) I + 2a \sum_{i=0}^{n-1} b_i Z_i + 2 \sum_{0 \leqslant i < j \leqslant n-1} b_i b_j\, Z_i Z_j, \tag{3.5}$$

with $a = (1/2)(2^n - 1)$, $b_i = -(1/2) \times 2^{n-i-1}$ and Z_i is the Pauli-Z gate applied to qubit i. Based on this, $\hat{x} = (0, 1, 2, 3, \ldots)$ and $\hat{x}^2 = (0, 1, 4, 9, \ldots)$ are diagonal matrices. The commutation relation between the individual terms can be used to make the measurement more efficient and the results of $\langle x\rangle = \langle\psi|\hat{x}|\psi\rangle$, $\langle x^2\rangle = \langle\psi|\hat{x}^2|\psi\rangle$ can then be linearly rescaled to be compatible with the wavefunction domain in energy γ.

4. Conclusions

In this work, we present a quantum-hybrid algorithm approach to the quantum radiation reaction, providing similar results when benchmarked against the particle-in-cell Monte Carlo (PIC-MC) code `OSIRIS`. We have simulated the Fokker–Planck equation describing the stochastic cooling of an electron population in a strong magnetic field using the variational quantum imaginary time evolution (VarQITE) algorithm, showing good agreement with the results from PIC-MC. We have developed a new variational ansatz that mimics a Gaussian trial-function, capturing the first and second moments of the distribution functions while requiring fewer parameters than more general variational ansätze, by enforcing a parity symmetry on

https://doi.org/10.1017/S0022377825100652 Published online by Cambridge University Press

the wavefunction in addition to a direct control on its average position through the advection operator. We have also derived closed-form analytical results for moments of the energy distribution functions, their entropy and autocorrelation functions.

Future steps will include extending this approach to other Fokker–Planck equations of interest (for example, the Kompaneets equation or laser cooling of trapped atoms), to the full Boltzmann equation (non-local operator) and to represent the quantum system not as a classical distribution function but as a Fock state (Hidalgo & Draper 2024), where the dynamics would be naturally unitary. Additionally, using specialised circuits for loading specific distribution functions as part of the variational ansatz (Gaussian, uniform, Chi-squared) could lead to a reduced number and more interpretable parameters, which would speed up the VarQITE algorithm and possibly mitigate the barren plateau problem.

Our work can contribute to further development of both classical diffusive plasma physics and to simulate the fully quantum nature of plasma interactions, namely the transition from semi-classical to non-perturbative SFQED regimes.

Acknowledgments

The authors thank the anonymous referees for their insightful comments and suggestions, which have significantly contributed to enhancing the clarity and rigor of this work. The authors also thank the following people for fruitful discussions / proofreading parts of the manuscript: Mr José Mariano on Monte Carlo sampling, Mr Lucas Ansia on classical simulation of the Fokker–Planck equation, Mr Bernardo Barbosa on the quantum radiation reaction in SFQED, Mr Pablo Bilbao on plasma dynamics in strong magnetic fields, Mr Gabriel Almeida on expressibility and complexity of variational quantum circuits, Mr Anthony Gandon on efficient Pauli-String decomposition of Hamiltonians for variational quantum circuits, Mr Efstratios Koukoutsis on Lindbladian/dissipative quantum simulations and Mr Diogo Cruz on quantum algorithms for PDE solvers. Simulations were performed at the IST cluster (Lisbon, Portugal). We have used the quantum frameworks Qiskit (Javadi-Abhari *et al*. 2024) and PennyLane (Bergholm *et al*. 2022).

Editor Nuno Loureiro thanks the referees for their advice in evaluating this article.

Declaration of interest

The authors report no conflict of interest.

Funding

This work was supported by the Portuguese Science Foundation (FCT) Grants Nos. PTDC/FIS-PLA/3800/2021, UI/BD/153735/2022. This work has been carried out within the framework of the EUROfusion Consortium, funded by the European Union via the Euratom Research and Training Programme (Grant Agreement No. 101052200 – EUROfusion). Views and opinions expressed are however those of the authors only and do not necessarily reflect those of the European Union or the European Commission. Neither the European Union nor the European Commission can be held responsible for them.

Data availability

The data that support the findings of this study are openly available at the following URL/DOI: https://github.com/OsAmaro/QuantumFokkerPlanck.

The repository includes notebooks explaining the classical PDE solver, the VarQITE approach, the analytical models and input decks for `OSIRIS` simulations.

Appendix A. Applying the variational principle to the heat equation

In this appendix, we provide a step-by-step application of McLachlan's variational principle (MVP) to the simplest diffusive PDE, the heat equation. Similar to the classical variational principle used in quantum mechanics to obtain approximate ground states of a system, the MVP for imaginary or real-time evolution is useful both numerically and analytically.

The one-dimensional (1-D) homogeneous heat equation

$$\partial_t u = k\, \partial_{xx} u \tag{A.1}$$

with thermal diffusivity coefficient k, admits a kernel solution (when $u(t=0, x) = \delta(x)$)

$$u(t, x) = \frac{1}{\sqrt{4\pi k t}} \exp\left(-\frac{x^2}{4kt}\right), \tag{A.2}$$

from which analytical solutions to more general initial conditions can be constructed.

This suggests using an ansatz

$$v(A, \sigma) = A \exp\left(-\frac{x^2}{2\sigma^2}\right), \quad \partial_t v = \hat{L}_H\, v, \tag{A.3}$$

with $\hat{L}_H$ the linear operator generating the evolution of the system (in this case, it is the Laplacian ∂_{xx}) and variational parameters $\theta_i(t) = (A(t), \sigma(t))$ for the analytical solution of the MVP. We take the thermal diffusivity to be $k = 1$ for simplicity. Since this function is L_1-normalised (that is, $\int v\, \mathrm{d}x = 1$), the normalisation A will be correlated and a function of the parameter σ.

The following derivatives and integrals are used in the calculations:

$$\partial_A v = A^{-1}\, v, \quad \partial_\sigma v = x^2\, \sigma^{-3}\, v, \quad \partial_{xx} v = v\, (x^2 - \sigma^2)\, \sigma^{-4},$$

$$\int v\, \mathrm{d}x = A\sqrt{2\pi}\sigma, \int v^2\, \mathrm{d}x = A^2\sqrt{\pi}\sigma, \tag{A.4}$$

$$\int x^2 v^2\, \mathrm{d}x = A^2\sqrt{\pi}\sigma^3/2, \int x^4 v^2\, \mathrm{d}x = 3A^2\sqrt{\pi}\sigma^5/4.$$

From the MVP (3.3), we need to compute the matrix elements $\int (\partial_k v)(\partial_j v)\, \mathrm{d}x$, which require either the $\int v^2\, \mathrm{d}x$ or $\int x^2\, v^2\, \mathrm{d}x$ integrals. We obtain

$$M_{A,A} = \sqrt{\pi}\sigma,\ M_{A,\sigma} = M_{\sigma,A} = \sqrt{\pi}A/2,\ M_{\sigma,\sigma} = 3\sqrt{\pi}A^2/(4\sigma).$$

For the column vector, we need to compute $\int (\partial_k v)(\hat{L}_H v)\, \mathrm{d}x$. We obtain

$$V_A = -A\sqrt{\pi}/(2\sigma), \quad V_\sigma = A^2\sqrt{\pi}/(4\sigma^2).$$

We now need to solve the matrix equation $M_{k,j}\dot{\theta}_j = V_k$. Factors of $\sqrt{\pi}$ will cancel out:

$$\begin{bmatrix} \sigma & A/2 \\ A/2 & 3A^2/(4\sigma) \end{bmatrix} \begin{bmatrix} \dot{A} \\ \dot{\sigma} \end{bmatrix} = V_k \leftrightarrow \begin{bmatrix} \dot{A} \\ \dot{\sigma} \end{bmatrix} = \begin{bmatrix} 3/(2\sigma) & -1/A \\ -1/A & 2\sigma/A^2 \end{bmatrix} \begin{bmatrix} -A/(2\sigma) \\ A^2/(4\sigma^2) \end{bmatrix} = \begin{bmatrix} -A/\sigma^2 \\ 1/\sigma \end{bmatrix}, \tag{A.5}$$

https://doi.org/10.1017/S0022377825100652 Published online by Cambridge University Press

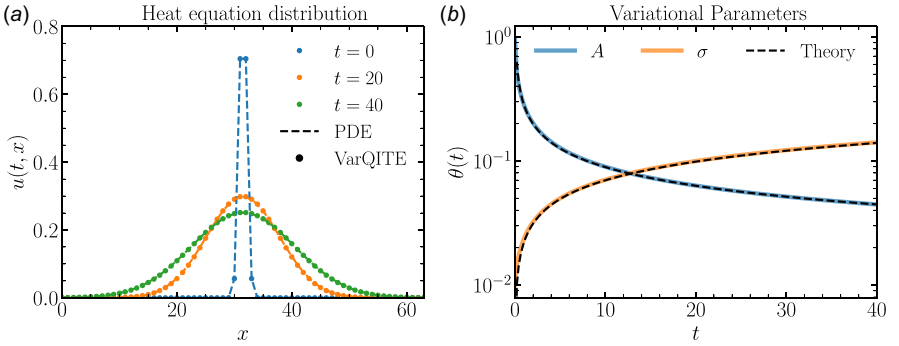

FIGURE 10. Numerical solution of the 1-D heat equation. (*a*) Snapshots of the distribution $u(t, x)$ from a PDE solver and numerical evolution of a Gaussian ansatz in the MVP. (*b*) Evolution of the variational parameters: colour, numerical MVP; dashed, analytical solution to the MVP (A.6).

where we explicitly computed the matrix inverse of $M_{k,j}$. The second equation (for σ) is separable. We can then replace $\sigma(t)$ in the first equation to obtain the amplitude $A(t)$. The parameters thus become

$$\sigma(t) = \sqrt{2t + \sigma_0^2},\ A(t) = A_0\sigma_0/\sqrt{2t + \sigma_0^2}, \tag{A.6}$$

where σ_0, A_0 are the initial spread and amplitude, respectively. This is precisely the exact analytical solution (A.2). In figure 10, we show a comparison between a standard PDE solver solution of the heat equation, a numerical solution of the MVP equations using the ansatz (A.3) (without a quantum circuit), and the analytical solution (A.6). The numerical grid had 2^6 cells, the number of time steps was 200 for a maximum simulation time of 40 and a small initial spread of the distribution function $\sigma_0 = 0.01$.

Appendix B. The Fokker–Planck equation

B.1. *Review of theoretical study of radiation reaction*

In this section, we review past works on the radiation reaction, introduce the main parameters that describe the interaction of electrons with an intense magnetic field and derive analytical solutions for some observables of interest. In the past decades, the theoretical modelling of electron radiation losses in intense fields has been extensively studied. Shen & White (1972) derive the transport partial differential equation (PDE) for electrons in a constant uniform magnetic field. Analytical results of multi-photon scattering of electrons in periodic structures (e.g. oriented-crystals) have been derived by Khokonov (2004) and Bondarenco (2014); however, without simple explicit closed-form expressions for the observables, nor immediate application in electron-laser scattering. Lobet *et al.* (2016) numerically studied the coupled dynamics of photons and leptons, including radiation reaction and pair production in a constant magnetic field. Vranic *et al.* (2016), Ridgers *et al.* (2017) and Niel *et al.* (2018) derive the ordinary differential equations (ODEs) for the first two momenta of the energy distributions of electrons interacting with a laser pulse, but do not present their corresponding closed-form explicit solutions. Niel *et al.* (2018) show connections between the different regimes of radiation reaction

https://doi.org/10.1017/S0022377825100652 Published online by Cambridge University Press

and the corresponding particle trajectories and stochastic PDEs. Artemenko *et al.* (2019) numerically solved the electron transport PDE for different magnetic field values using the 'global constant field approximation' to map between a constant magnetic field set-up and a laser pulse with a finite duration envelope. Jirka *et al.* (2021) derive the average energy decay in a pulsed plane-wave laser in the highly 'nonlinear quantum' high-χ regime (the quantum nonlinear parameter, χ, is defined in § 2).

More recently, some papers have contributed with new analytical results for the study of classical (CRR) and quantum (QRR) radiation reaction regimes. Bilbao & Silva (2023) derive analytically the evolution of an electron momentum 'ring distribution' in a maser set-up, relevant for astrophysical plasma scenarios. The formulae are derived in the CRR regime using the 'method of lines' technique but appear to hold even for $\chi \sim 0.1$, and suggest that this class of ring distributions is a 'global attractor'. Zhang, Zhang & Zhou (2023) derive approximate analytical formulae for the evolution of a lepton distribution function in a constant magnetic field during multiphoton scattering in the QRR $\chi < 1$ regime. The authors identify and analytically characterise the 'quantum peak splitting', which occurs when an initially peaked distribution function evolves into a doubly peaked distribution. Bulanov *et al.* (2024) derive CRR closed-form expressions for distribution functions for a set of initial conditions of interest, again using the 'method of lines', and find an equilibrium (time-independent) solution for the QRR Fokker–Planck equation of an electron beam in an LWFA set-up. Kostyukov *et al.* (2023) derive short-time evolution expressions for the electron wave packet in a strong EM field, including the expectation value of the electron spin. The approach relies on Volkov functions and the Dyson–Schwinger equation, and naturally leads to the damping (radiation reaction) of the wave packet. Torgrimsson (2024*a*,*b*) derives explicit analytical time-dependent electron distribution functions in momentum and spin through resummation techniques. Following a similar approach, Blackburn (2024) derives explicit analytical QRR formulae for the final electron mean energy and spread as functions of initial electron energy, laser a_0 and pulse duration. These expressions are derived in the low-χ regime, but remain approximately valid for a larger range of parameters.

B.2. *Regimes of radiation reaction*

Here, we follow the notation of Vranic *et al.* (2016). When $\chi \ll 1$, the equation for energy loss can be derived from the Landau–Lifshitz equation, leading to

$$\frac{\mathrm{d}\gamma}{\mathrm{d}t} = -c_{rr}\,\gamma^2, \tag{B.1}$$

with $c_{rr} \equiv 2\,\omega_c e^2 b_0^2/(3mc^3)$ a constant defining the effect of classical radiation reaction. In the set-up considered, three physical parameters completely describe the dynamics: the initial electron energy γ_0, the external magnetic field B and the evolution time t. The solution for the energy is

$$\gamma_c(t) \sim \gamma_0/(1 + c_{rr}\,t\,\gamma_0). \tag{B.2}$$

This scaling for the average energy can be corrected in the $\chi \lesssim 1$ regime.

From a distribution point of view, the relativistic Vlasov equation for the electron distribution function f is modified. The radiation reaction no longer preserves

https://doi.org/10.1017/S0022377825100652 Published online by Cambridge University Press

phase-space volume, corresponding to the operator on the right-hand side of the equation

$$\frac{\mathrm{d}f(t,\vec{x},\vec{p})}{\mathrm{d}t} = \frac{\partial f}{\partial t} + v\cdot\nabla_x f + F\cdot\nabla_p f = \mathcal{C}[f_e], \tag{B.3}$$

where $\mathcal{C}$ is a collision operator whose form depends on the model/regime of radiation reaction considering Niel *et al.* (2018). In our simplified set-up, the coordinate gradient and the force terms vanish, so the only term of interest is the collision operator.

For higher values of χ, the emission of photons becomes stochastic, in general, leading to a spread in energy. Conceptually, the electrons can be thought of as being slightly scattered through a cloud of photons of the field, where each photon has an energy much lower than that of the electron.

There are several approximation methods for the theoretical analysis and numerical sampling of the cross-sections contained in the collision operator $\mathcal{C}$. One of the most commonly used is the locally constant field approximation (LCFA), which is exact for a plane wave laser field, and where the electric, magnetic and Poynting vectors are mutually orthogonal.

Within this approximation, the probability of emission of a photon with χ_γ by an electron with χ per unit time, also known as the nonlinear Compton scattering (nCS) differential cross-section/rate, is

$$\frac{\mathrm{d}^2 N_\gamma}{\mathrm{d}t\ \mathrm{d}\chi_\gamma}(\chi,\chi_\gamma) = \frac{\alpha mc^2}{\sqrt{3}\pi\hbar\gamma\chi}\left[\left(1-\xi+\frac{1}{1-\xi}\right)K_{2/3}(\tilde{\chi}) - \int_{\tilde{\chi}}^{\infty} K_{1/3}(x)\,\mathrm{d}x\right] \tag{B.4}$$

with $\xi \equiv \chi/\chi_\gamma$, $\tilde{\chi} \equiv 2\xi/(3\chi(1-\xi))$ and K_n is the modified Bessel function of second kind (Abramowitz & Stegun 1964). This rate in χ_γ can be mapped to a rate in particle energy $\mathrm{d}^2N_\gamma/\mathrm{d}t\,\mathrm{d}\gamma_\gamma$ (γ,γ_γ).

In the LCFA approximation, the Lorentz invariant is $E^2 - B^2 = 0$. In the case of a constant magnetic field, the boosted electromagnetic field in the electron rest frame is almost a perfect plane wave, with a very slight deviation from this approximation. The result is that the nCS and the quantum synchrotron emission spectra for ultra-relativistic leptons are in practice very similar, as can be confirmed by Niel *et al.* (2018) and Zhang *et al.* (2023).

The Fokker–Planck (FP) equation can be seen as an extension of the standard Vlasov equation to kinetically and stochastically model collisions between plasma species and laser–plasma interaction. An important application is simulating the energy loss of an electron beam as it interacts with electromagnetic fields (Neitz & Di Piazza 2013; Vranic *et al.* 2016). In this case, the particle distribution evolves through

$$\frac{\partial f(t,\vec{p})}{\partial t} = \frac{\partial}{\partial p_l}\left[-\mathcal{A}_l f + \frac{1}{2}\frac{\partial}{\partial p_k}(\mathcal{B}_{lk} f)\right] \tag{B.5}$$

with $\mathcal{A}_l \equiv \int q_l w(\vec{p},\vec{q})\mathrm{d}^3\vec{q}$, $\mathcal{B}_{lk} \equiv \int q_l q_k w(\vec{p},\vec{q})\mathrm{d}^3\vec{q}$, the drift and diffusion coefficients, respectively, and $w(\vec{p},\vec{q})\,\mathrm{d}^3\vec{p}$ is the probability per unit time of momentum change of the electron $\vec{p}\to\vec{p}-\vec{q}$, with $\vec{q}$ the momentum of the photon, and where Einstein index contraction was assumed.

In the co-linear approximation of radiation emission, $\chi_\gamma/\chi \sim \hbar k/(\gamma mc)$, this problem becomes essentially 1-D, with drift and diffusion coefficients

$$\mathcal{A} \equiv \frac{\gamma mc}{\chi}\int_0^\chi \chi_\gamma \frac{\mathrm{d}^2N_\gamma}{\mathrm{d}t\,\mathrm{d}\chi_\gamma}\,\mathrm{d}\chi_\gamma, \quad \mathcal{B} \equiv \frac{(\gamma mc)^2}{\chi^2}\int_0^\chi \chi_\gamma^2 \frac{\mathrm{d}^2N_\gamma}{\mathrm{d}t\,\mathrm{d}\chi_\gamma}\,\mathrm{d}\chi_\gamma. \tag{B.6}$$

https://doi.org/10.1017/S0022377825100652 Published online by Cambridge University Press

In the regime of $\chi \ll 1$, the $\mathcal{A}$ and $\mathcal{B}$ coefficients have polynomial approximations (Vranic *et al.* 2016)

$$\mathcal{A} \sim \frac{2}{3}\frac{\alpha m^2 c^3}{\hbar}\chi^2 \propto \gamma^2, \quad \mathcal{B} \sim \frac{55}{24\sqrt{3}}\frac{\alpha m^3 c^4}{\hbar}\gamma\,\chi^3 \propto \gamma^4. \tag{B.7}$$

The Fokker–Planck equation is sparse (only two local, differential operators), while the Boltzmann equation is non-local and its corresponding Hamiltonian evolution matrix is dense. Consequently, both numerical (either a PDE solver or Monte Carlo sampling) and analytical solutions of the latter equation are often more challenging than for the former.

B.3. *Entropy and autocorrelation*

Having derived the evolution of the spread (2.6) and assuming a Gaussian functional form of the distribution function, the Shannon entropy of the electron beam evolves as $S(t) = -\int f \log(f)\,\mathrm{d}\gamma \sim \log(\sigma(t)) + c^{te}$ up to an additive constant (which we choose such that the simulation and theory curves match at late times). Since this is a monotone function of the spread, it has the same qualitative behaviour and peaks at $\log(\sigma_{\max})$. From a physics point-of-view, the entropy changes due to a competition between the drift and diffusion processes. At late times, the entropy of the electrons decreases, which can be interpreted as a transfer of entropy to the radiation that is being emitted.

One can also compute an approximate auto-correlation function $g(\tau)$ (not to be confused with the gaunt factor) from the classical solution $\gamma_c(t) \sim \gamma_0/(1 + 2R_c t/3)$ as

$$g(\tau) \equiv \frac{\langle \gamma(t)\gamma(t+\tau)\rangle}{\langle \gamma^2(t)\rangle} = \int_0^\infty \frac{1}{(1+2R_c t/3)(1+2R_c(t+\tau)/3)}\,\mathrm{d}t \propto \frac{\log(1+2R_c\tau/3)}{2R_c\tau/3}, \tag{B.8}$$

where normalisation $g(0) = 1$ is enforced. This quantifies how correlated two electron trajectories are on average if measured with a time delay of τ. Using instead the second-order expansion for the average energy (that is, the full (2.5)) leads to a more accurate closed-form solution, albeit with more terms (not shown here). Considering the stochastic component of the trajectories would require computing expectation values of nonlinear functions of Wiener processes $W(t)$, $W(t+\tau)$. The solution to the Fokker–Planck equation $f(t, \gamma)$ does not give us information on the auto-correlation directly, and a marginal distribution $f(t_1, \gamma_1; t_2, \gamma_2)$ would have to be obtained.

In figure 11, we show the comparison between these two quantities $S(t)$, $g(\tau)$ from OSIRIS simulations computed from distribution histograms and individual particle trajectories, and the approximate analytical results. Again, for $\chi_0 = 10^{-1}$ (blue curve), the t-axis is again multiplied by a factor of 2 to have the same range as the other curves.

B.4. *McLachlan's variational principle approach*

Here, we apply the technique described in Appendix A to the Fokker–Planck equation. Since the number of particles (L_1 norm) is conserved and we are mostly

https://doi.org/10.1017/S0022377825100652 Published online by Cambridge University Press

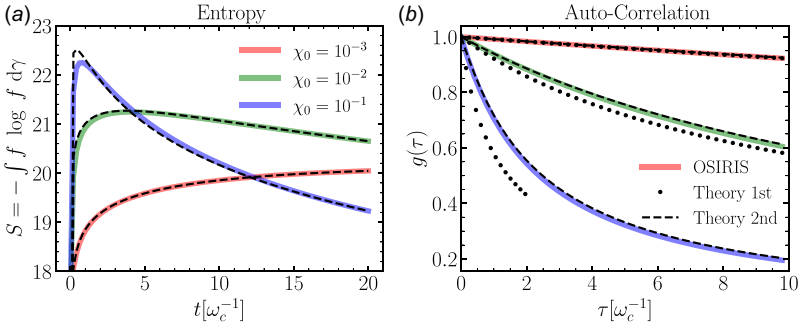

FIGURE 11. (*a*) Evolution of the distribution function entropy, (*b*) auto-correlation function, where dotted lines represent (B.8) and dashed lines are the result of using (2.5) in $g(\tau)$. In both figures, coloured lines represent results from OSIRIS simulations.

interested in the first moments of the distribution function $\mu = \int \gamma f \, d\gamma$, $\sigma^2 = \int (\gamma - \mu)^2 f \, d\gamma$, we enforce this into the ansatz

$$v(\mu, \sigma) = \frac{1}{\sqrt{2\pi\sigma^2}} \exp\left(-\frac{(\gamma-\mu)^2}{2\sigma^2}\right), \quad \partial_t v = \hat{L}_{FP}\, v = -\partial_\gamma (a\, \gamma^2\, v) + 0.5\, \partial_{\gamma\gamma}(b\, \gamma^4\, v), \tag{B.9}$$

with $\hat{L}_{FP}$ the linear operator generating the dynamics, and variational parameters $\theta_i(t) = (\mu(t), \sigma(t))$, for the analytical solution of the MVP. We could have used an ansatz with the amplitude $A(t)$, which would have led to a 3×3 matrix system of equations.

The following derivatives will be used in the following calculations:

$$\frac{\partial_\mu v}{v} = \frac{\gamma - \mu}{\sigma^2}, \qquad \frac{\partial_\sigma v}{v} = \frac{(\gamma-\mu)^2 - \sigma^2}{\sigma^3}. \tag{B.10}$$

From the MVP (3.3), we need to compute the matrix elements $\int (\partial_k v)(\partial_j v) d\gamma$, which require either the $\int (\gamma-\mu)^2\, v^2\, d\gamma$ or the $\int (\gamma-\mu)^4\, v^2\, d\gamma$ Gaussian integrals. In general, the change of variables $(\gamma - \mu)/\sigma \to \gamma$ simplifies the calculations. We obtain

$$M_{\mu\mu} = 1/(4\sqrt{\pi}\sigma^3), \quad M_{\sigma\sigma} = 3/(8\sqrt{\pi}\sigma^3), \quad M_{\mu\sigma} = M_{\sigma\mu} = 0,$$

where the cross-term is null due to the odd-symmetry of the integrand function. The diagonal structure of this matrix simplifies the calculations considerably. The inverse matrix becomes

$$M_{kj}^{-1} = 4\sqrt{\pi}\sigma^3 \begin{bmatrix} 1 & 0 \\ 0 & 2/3 \end{bmatrix}. \tag{B.11}$$

For the column vector, we obtain

$$V_\mu = \frac{a(-2\mu^2 + \sigma^2)}{8\sqrt{\pi}\sigma^3} - \frac{3b\mu(2\mu^2 + \sigma^2)}{8\sqrt{\pi}\sigma^3},$$

$$V_\sigma = -\frac{3a\mu}{4\sqrt{\pi}\sigma^2} - \frac{3b(-4\mu^4 + 36\mu^2\sigma^2 + 13\sigma^4)}{64\sqrt{\pi}\sigma^3}.$$

https://doi.org/10.1017/S0022377825100652 Published online by Cambridge University Press

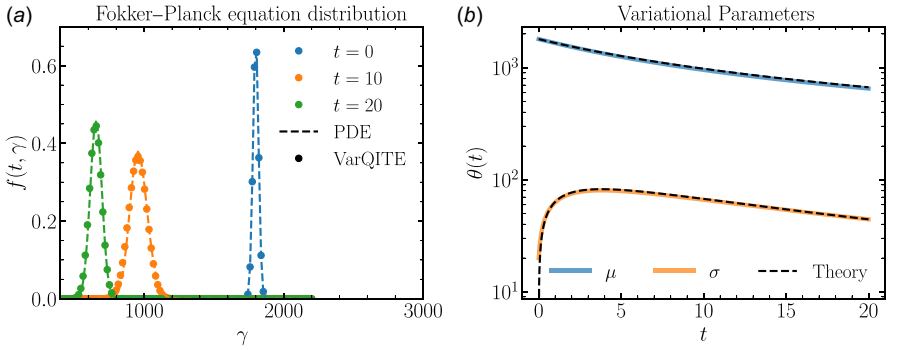

FIGURE 12. Numerical simulation of the Fokker–Planck equation with $\chi_0 = 10^{-2}$. (*a*) Evolution of the distribution function $f(t, \gamma)$. The dashed line represents the result from a standard PDE solver, while circles represent the numerical integration of the MVP equations. (*b*) Evolution of the moments and variational parameters (μ, σ). The coloured lines represent the moments of the distribution function obtained from the PDE solver, while dashed lines represent the analytical results of (2.5) and (2.6).

Applying the inverse matrix M_{kj}^{-1} to the column vector V_k, we obtain

$$\begin{bmatrix} \dot{\mu} \\ \dot{\sigma} \end{bmatrix} = \begin{bmatrix} \underline{-a\mu^2 + a\sigma^2/2} - 3b\mu(2\mu^2 + \sigma^2)/2 \\ \underline{-2a\mu\sigma + b\mu^4/(2\sigma)} - b(36\mu^2\sigma^2 + 13\sigma^4)/(8\sigma) \end{bmatrix}. \tag{B.12}$$

Changing notation $2\alpha_{rr} = a$ and $b\mu^4 = B/(m^2c^2)$, the underlined terms, which are leading order assuming $\mu \gg \sigma$, recover the results of (8) and (14) from Vranic *et al.* (2016).

In figure 12, we show a comparison between a PDE solver solution of the Fokker–Planck equation, a numerical solution of the MVP-VarQITE equations using the ansatz (B.9) (without a quantum circuit), and the analytical solution (2.5). The numerical grid had 2^7 cells, the number of time steps was 900 for a maximum simulation time of 20, $\chi_0 = 10^{-2}$ and initial momenta $\mu_0 = 1800$, $\sigma_0 = 20$. We have thus shown the potential of MVP for retrieving the distribution moments in the quantum radiation reaction.

REFERENCES

ABRAMOWICZ, H., *et al.* 2021 Conceptual design report for the LUXE experiment. *Eur. Phys. J. Spec. Top.* **230**, 2445–2560.

ABRAMOWICZ, H., *et al.* 2019 Letter of intent for the LUXE experiment. arXiv:1909.00860.

ABRAMOWITZ, M. & STEGUN, I. A. 1964 *Handbook of Mathematical Functions with Formulas, Graphs, and Mathematical Tables*. U.S. Government Printing Office.

ALGHASSI, H., DESHMUKH, A., IBRAHIM, N., ROBLES, N., WOERNER, S. & ZOUFAL, C. 2022 A variational quantum algorithm for the Feynman-Kac formula. *Quantum* **6**, 730.

AMARO, ÓSCAR & CRUZ, D. 2023 A living review of quantum computing for plasma physics. arXiv:2302.00001.

ARTEMENKO, I. I., KRYGIN, M. S., SEREBRYAKOV, D. A., NERUSH, E. N. & KOSTYUKOV, I. Y. 2019 Global constant field approximation for radiation reaction in collision of high-intensity laser pulse with electron beam. *Plasma Phys. Contr. F.* **61**, 074003.

BERGHOLM, V., *et al.* 2022 PennyLane: Automatic differentiation of hybrid quantum-classical computations. arXiv:1811.04968.

https://doi.org/10.1017/S0022377825100652 Published online by Cambridge University Press

BILBAO, P. J. & SILVA, L. O. 2023 Radiation reaction cooling as a source of anisotropic momentum distributions with inverted populations. *Phys. Rev. Lett.* **130**, 165101.

BLACKBURN, T. G. 2024 Analytical solutions for quantum radiation reaction in high-intensity lasers. *Phys. Rev. A* **109**, 022234.

BONDARENCO, M. V. 2014 Multiphoton effects in coherent radiation spectra. *Phys. Rev. D* **90**, 013019.

BULANOV, S. V., GRITTANI, G. M., SHAISULTANOV, R., ESIRKEPOV, T. Z., RIDGERS, C. P., BULANOV, S. S., RUSSELL, B. K. & THOMAS, A. G. R. 2024 On the energy spectrum evolution of electrons undergoing radiation cooling. *Fundam. Plasma Phys.* **9**, 100036.

COLE, J. M., *et al.* 2018 Experimental evidence of radiation reaction in the collision of a high-intensity laser pulse with a laser-wakefield accelerated electron beam. *Phys. Rev. X* **8**, 011020.

CRUZ, F., GRISMAYER, T., CHEN, A. Y., SPITKOVSKY, A. & SILVA, L. O. 2021 Coherent emission from QED cascades in pulsar polar caps. *Astrophys. J. Lett.* **919**, L4.

DASGUPTA, K. & PAINE, B. 2022 Loading probability distributions in a quantum circuit. arXiv:2208.13372.

DODIN, I. Y. & STARTSEV, E. A. 2021 On applications of quantum computing to plasma simulations. *Phys. Plasmas* **28**, 092101.

ELI Extreme Light Infrastructure. https://eli-laser.eu/.

ENDO, S., SUN, J., LI, Y., BENJAMIN, S. C. & YUAN, X. 2020 Variational quantum simulation of general processes. *Phys. Rev. Lett.* **125**, 010501.

ENGEL, A., SMITH, G. & PARKER, S. E. 2019 Quantum algorithm for the Vlasov equation. *Phys. Rev. A* **100**, 062315.

FACET-II. https://facet-ii.slac.stanford.edu/facility.

FARHI, E., GOLDSTONE, J. & GUTMANN, S. 2014 A quantum approximate optimization algorithm. arXiv:1411.4028.

FONSECA, R. A., *et al.* 2002 OSIRIS: a three-dimensional, fully relativistic particle in cell code for modeling plasma based accelerators. In *Computational Science – ICCS. 2002* (ed. Sloot, P. M. A., Hoekstra, A. G., Tan, C. J. K. & Dongarra), J. J.), pp. 342–351, Springer.

HARRIS, C. R., *et al.* 2020 Array programming with numPy. *Nature* **585**, 357–362.

HIBEF. https://www.hzdr.de/db/Cms?pOid=51491&pNid=711&pLang=en.

HIDALGO, L. & DRAPER, P. 2024 Quantum simulations for strong-field QED. *Phys. Rev. D* **109**, 076004.

JAVADI-ABHARI, A., *et al.* 2024 Quantum computing with Qiskit. arXiv:2405.08810.

JIRKA, M., SASOROV, P., BULANOV, S. S., KORN, G., RUS, B. & BULANOV, S. V. 2021 Reaching high laser intensity by a radiating electron. *Phys. Rev. A* **103**, 053114.

JOSEPH, I., SHI, Y., PORTER, M. D., CASTELLI, A. R., GEYKO, V. I., GRAZIANI, F. R., LIBBY, S. B. & DUBOIS, J. L. 2023 Quantum computing for fusion energy science applications. *Phys. Plasmas* **30**, 010501.

KHOKONOV, M. K. 2004 Cascade processes of energy loss by emission of hard phonons. *J. Exp. Theor. Phys.* **99**, 690–707.

KOSTYUKOV, I. Y., NERUSH, E. N., MIRONOV, A. A. & FEDOTOV, A. M. 2023 Short-term evolution of electron wave packets in constant crossed electromagnetic fields with radiative corrections. *Phys. Rev. D* **108**, 093007.

KUBO, K., NAKAGAWA, Y. O., ENDO, S. & NAGAYAMA, S. 2021 Variational quantum simulations of stochastic differential equations. *Phys. Rev. A* **103**, 052425.

LIU, J., LI, Z. & YANG, J. 2024 Perturbative variational quantum algorithms for material simulations. *Electronic Structure* **6**, 015007.

LOBET, M., D'HUMIÈRES, E., GRECH, M., RUYER, C., DAVOINE, X. & GREMILLET, L. 2016 Modeling of radiative and quantum electrodynamics effects in PIC simulations of ultra-relativistic laser-plasma interaction. *J. Phys.: Confer. Ser.*, **688**, 012058.

LOS, E. E., *et al.* 2024, Observation of quantum effects on radiation reaction in strong fields. arXiv:2407.12071.

MCLACHLAN, A. D. 1964 A variational solution of the time-dependent Schrodinger equation. *Mol. Phys.* **8**, 39–44.

https://doi.org/10.1017/S0022377825100652 Published online by Cambridge University Press

MEDIN, Z. & LAI, D. 2010 Pair cascades in the magnetospheres of strongly magnetized neutron stars. *Mon. Not. R. Astron. Soc.* **406**, 1379–1404.

MEUREN, S., BUCKSBAUM, P. H., FISCH, N. J., FIÚZA, F., GLENZER, S., HOGAN, M. J., QU, K., REIS, D. A., WHITE, G. & YAKIMENKO, V. 2020 In *On seminal HEDP research opportunities enabled by colocating multi-Petawatt laser with high-density electron beams*. arXiv:2002.10051.

NEITZ, N. & DI PIAZZA, A. 2013 Stochasticity effects in quantum radiation reaction. *Phys. Rev. Lett.* **111**, 054802.

NIEL, F., RICONDA, C., AMIRANOFF, F., DUCLOUS, R. & GRECH, M. 2018 From quantum to classical modeling of radiation reaction: a focus on stochasticity effects. *Phys. Rev. E* **97**, 043209.

NIELSEN, M. A. & CHUANG, I. L. 2010 *Quantum Computation and Quantum Information: 10th Anniversary Edition*. Cambridge University Press.

NSF-OPAL. https://www.lle.rochester.edu/index.php/omega-laser-facility-2/.

PAPADOPOULOS, D. N., ZOU, J. P. & LE BLANC, C. 2016 & others 2016 the Apollon 10 PW laser: experimental and theoretical investigation of the temporal characteristics. *High Power Laser Science and Engineering* **4**, e34.

PERUZZO, A., MCCLEAN, J., SHADBOLT, P., YUNG, M.-H., ZHOU, X.-Q., LOVE, P. J., ASPURU-GUZIK, A. & O'BRIEN, J. L. 2014 A variational eigenvalue solver on a photonic quantum processor. *Nat. Commun.* **5**, 4213.

PODER, K., *et al.* 2018 Experimental signatures of the quantum nature of radiation reaction in the field of an ultraintense laser. *Phys. Rev. X* **8**, 031004.

PRESKILL, J. 2018 Quantum computing in the NISQ era and beyond. *Quantum* **2**, 79.

RIDGERS, C. P., *et al.* 2017 Signatures of quantum effects on radiation reaction in laser–electron-beam collisions. *J. Plasma Phys.* **83**, 715830502.

ROBERT, A., BARKOUTSOS, P. K., WOERNER, S. & Tavernelli. Ivano 2021 Resource-efficient quantum algorithm for protein folding. *NPJ Quantum Inf.* **7**, 1–5.

SATO, Y., KONDO, R., HAMAMURA, I., ONODERA, T. & YAMAMOTO, N. 2024 Hamiltonian simulation for hyperbolic partial differential equations by scalable quantum circuits. *Phys. Rev. Res.* **6**, 033246.

SCHOEFFLER, K. M., GRISMAYER, T., UZDENSKY, D. & SILVA, L. O. 2023 High-energy synchrotron flares powered by strongly radiative relativistic magnetic reconnection: 2D and 3D PIC simulations. *Mon. Not. R. Astron. Soc.* **523**, 3812–3839.

SHEN, C. S. & WHITE, D. 1972 Energy straggling and radiation reaction for magnetic bremsstrahlung. *Phys. Rev. Lett.* **28**, 455–459.

SHI, Y., QIN, H. & FISCH, N. J. 2021 Plasma physics in strong-field regimes: theories and simulations. *Phys. Plasmas* **28**, 042104.

SIM, S., JOHNSON, P. D. & ASPURU-GUZIK, A. 2019 Expressibility and entangling capability of parameterized quantum circuits for hybrid quantum-classical algorithms. *Advanced Quantum Technologies* **2**, 1900070.

TIMOKHIN, A. N. 2010 Time-dependent pair cascades in magnetospheres of neutron stars – I. Dynamics of the polar cap cascade with no particle supply from the neutron star surface. *Mon. Not. R. Astron. Soc.* **408**, 2092–2114.

TORGRIMSSON, G. 2024a Qu*a*ntum radiation reaction: analytical approximations and obtaining the spectrum from moments. *Phys. Rev. D* **110**, 076012.

TORGRIMSSON, G. 2024b Quantum radiation reaction spectrum of electrons in plane waves. *Phys. Rev. D* **109**, 076030.

UZDENSKY, D. A. & RIGHTLEY, S. 2014 Plasma physics of extreme astrophysical environments. *Rep. Prog. Phys.* **77**, 036902.

VISSERS, G. & BOUTEN, L. 2019 Implementing quantum stochastic differential equations on a quantum computer. *Quantum Inf. Process.* **18**, 152.

VRANIC, M., GRISMAYER, T., FONSECA, R. A. & SILVA, L. O. 2016 Quantum radiation reaction in head-on laser-electron beam interaction. *New J. Phys.* **18**, 073035.

https://doi.org/10.1017/S0022377825100652 Published online by Cambridge University Press

MUKHIN, I., SOLOVIEV, A., PEREVEZENTSEV, E., SHAYKIN, A., GINZBURG, V., KUZMIN, I., MART'YANOV, M., SHAIKIN, I., KUZMIN, A., MIRONOV, S., YAKOVLEV, I., KHAZANOV, E. 2021 Design of the front-end system for a subexawatt laser of the XCELS facility, *Quantum Electronics* **51**, 759–767. doi: 10.1070/qel17620.

YOON, J. W., JEON, C., SHIN, J., LEE, S. K., LEE, H. W., CHOI, I. W., KIM, H. T., SUNG, J. H. & NAM, C. H. 2019 Achieving the laser intensity of 5.5 1022 W cm^{-1} with a wavefront-corrected multi-pw laser, *Opt. Express* **27**, 20412–20420.

ZEUS. https://zeus.engin.umich.edu.

ZHANG, B., ZHANG, Z.-M. & ZHOU, W.-M. 2023 Quantum splitting of electron peaks in ultra-strong fields. *Matter Radiat. Extremes* **8**, 054003.